

1 **PyIRI: Whole-Globe Approach to the International
2 Reference Ionosphere Modeling Implemented in
3 Python**

4 **Victoriya V. Forsythe¹, Dieter Bilitza^{1,2}, Angeline Burrell¹, Douglas P. Drob¹,
5 Kenneth Dymond¹, Bruce Fritz¹, Sarah McDonald¹**

6 ¹U.S. Naval Research Laboratory, Washington, DC, USA

7 ²Department of Physics and Astronomy, George Mason University, Fairfax, VA, USA

8 ³Heliospheric Laboratory, NASA Goddard Space Flight Center, Greenbelt, MD, USA

9 **Key Points:**

- 10 • Python tool for rapid global ionospheric electron density estimates
11 • Novel approach to CCIR coefficients and IRI model
12 • 24-hour global electron density in a few seconds

13 **Abstract**

14 International Reference Ionosphere model is widely used in the ionospheric community
 15 and considers to be an official standard for the empirical ionospheric models. The de-
 16 velopment of this model initiated in late 60th using FORTRAN language and punch card
 17 programming approach, where the model outputs are being calculated separately for each
 18 given geographic location and time stamp. The CCIR (and URSI) coefficients represent
 19 the skeleton of the IRI model, as they provide the global distribution of the maximum
 20 usable ionospheric frequency and M3000. At the U.S. Navy Research Laboratory (NRL)
 21 a novel Python tool was developed that enables global runs of IRI model that takes only
 22 several seconds. This became possible through the Python rebuild of the core IRI com-
 23 ponent that calculates ionospheric critical frequency using CCIR coefficients using ma-
 24 trix multiplication instead of cyclic addition. Additionally, the construction of the ver-
 25 tical electron density profiles in a matrix form were made possible by multidimensional
 26 *where* NumPy function. This paper explains in detail this new approach and introduces
 27 all components of the PyIRI package.

28 **Plain Language Summary**

29 International Reference Ionosphere (IRI) estimates the number of electrons in the
 30 upper atmosphere, which is important to know for the high frequency (HF) communi-
 31 cation and radio signal propagation. Scientists and communication specialists often use
 32 IRI to plan future and ongoing communication links. The IRI model, was written in late
 33 60th, when arrays and matrices were not fully used due to the punch-card approach to
 34 programming. For example, IRI evaluates electron density at each geographic location
 35 separately. This why it takes a long time to run IRI for high-resolution global grids. We
 36 introduced modern programming approaches to IRI code and built a Python tool PyIRI
 37 that enables estimation of the electron density for all grid points simultaneously. With
 38 PyIRI it takes just a few seconds to obtain the electron density for the entire global grid
 39 and for the duration of the entire day.

40 **1 Introduction**

41 The ionosphere is a region above the atmosphere that surrounds the Earth start-
 42 ing from 90 km of altitude and extending all the way up to 2,000 km. Unlike the neu-
 43 tral atmosphere, the ionosphere has free electrons that refract the electromagnetic waves,

especially the waves that have frequency below 300 MHz. Therefore, in order to establish the high frequency (HF) communication link between any two positions it is crucial to know the amount of the electrons along the signal path. The International Reference Ionosphere (IRI) empirical model can predict the electron density in the ionosphere based on the statistical analysis of the long data record and the ionospheric climatology.

The International Standardization Organization, the International Union of Radio Science, the Committee on Space Research, and the European Cooperation for Space Standardization have recognized IRI as the official standard for the Earth's ionosphere (ISO 16457: <https://www.iso.org/standard/61556.html>). A recent review paper by Bilitza et al. (2022) describes the current state of the IRI model, its history, and recent developments.

Despite being golden standard of the ionospheric modeling, the IRI software was developed in late 60th, using FORTRAN programming language and punch card programming approach, suitable during that period of time. As a result, the current execution of the IRI code is based on the sequential calculation of the electron density for each location on the globe and for each time step separately. As an example, to obtain the global density distribution during 24-hours, one needs to execute the IRI model $N_G \times N_T$ times, where N_G is the number of horizontal locations, and N_T is the number of diurnal time frames. Considering a typical global regular grid of $1^\circ \times 1^\circ$ and 15-min temporal resolution, the number of executions is equal to 6,272,736. Further imagine that one needs to analyze different seasonal dependencies, different solar conditions, or (a nightmare) to construct an ensemble of the global density distributions. This was a motivation to rethink and rebuild the current IRI approach to obtain the electron density, developing a software that allows for the simultaneous calculation of the electron density on the entire globe and during the entire day. It involves the total rebuild of the IRI core, namely the calculation of the $NmF2$ and $hmF2$ parameters from the CCIR (or URSI) coefficients. In other words, what previously required 6,272,736 executions is now possible to obtain in only one step (that takes only several seconds on a regular PC).

The focus of this paper is on the global and rapid construction of the main core of the IRI model, which is the climatology of the ionospheric peak density $NmF2$ and its height $hmF2$. These parameters represent the skeleton of the model, whereas all other parameters required to construct the vertical electron density profile (EDP) can be de-

rived from $NmF2$ and $hmF2$. The full version of the IRI model contains many options for the other parameters. For example, the parameters that describe the top side of the electron density profile (EDP) can be derived using 3 different approaches (Bilitza et al., 2022). This work will further present the construction of the EDP choosing the easiest approach, and, sometimes, even simplifying some traditional IRI methods, to keep the focus of the paper on the core of the IRI program.

Additionally, it is important to mention that there exist a few previously developed Python IRI wrappers and interfaces, e.g. `iri2016`, `pyiri2016`, and `pyglow`. However, they still use the original FORTRAN IRI code, making its execution more convenient for Python users. This work, on contrary, introduces a novel software that redefines the core of the IRI fully in Python language.

The rest of the paper: discusses a core of the IRI model or the use of the CCIR coefficients to obtain the main ionospheric parameters, introduces a novel approach to construct the global maps of $NmF2$ and $hmF2$, describes the derivation of other IRI components, and introduces a novel Python IRI software package that was made available to the community.

2 The core parameters of the IRI model

Despite a wide range of the different IRI options and internal sub-models, there are only three main parameters that work as independent anchor points for the construction of the ionospheric EDP. An example of the EDP is shown in Figure 1, where the independent variation of the three anchor points are visualized with arrows. The peak of the F2 region $NmF2$ and its height $hmF2$, are the two anchor points that determine the position of the F2 region. The peak of the E region NmE controls the shape of the E region, whereas the height of the peak is considered to be a constant value of 110 km. All other parameters that determine the shape of the EDP, such as the position and the peak density of the F1 region and the thicknesses of the F2, F1, and E regions can be determined from $NmF2$, $hmF2$, and NmE .

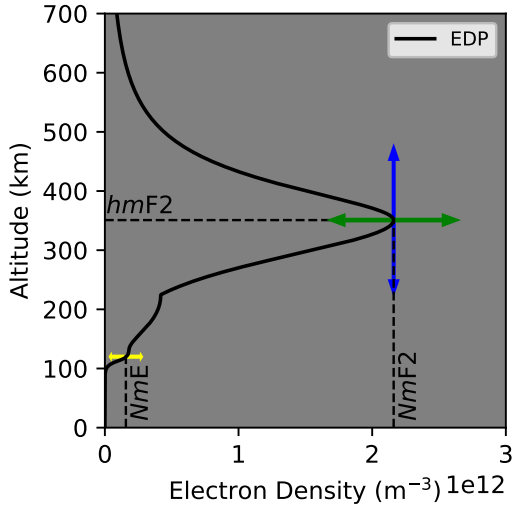


Figure 1. Three anchor points control the shape of the electron density profile, where the peak of the F2 region is determined by the $NmF2$ value, the height of the peak is determined by $hmF2$ parameter, and the peak of the E region is described by NmE with fixed height.

103 2.1 The peak of F2 region $NmF2$: traditional IRI approach

104 The IRI model, as well as NeQuick (Nava et al., 2008) model, employs the Con-
 105 sultative Committee on International Radio (CCIR) coefficients to obtain the diurnal
 106 and geographical variations of the ionospheric critical frequency $foF2$, whereas the $NmF2$
 107 is further derived from $foF2$ using the plasma physics formula

$$NmF2/m^{-3} = 0.124 \times 10^{11} (foF2/\text{MHz})^2. \quad (1)$$

108 The CCIR coefficients were obtained in the pioneered studies conducted by Jones
 109 and Gallet (1962, 1965); Jones et al. (1969). They analyzed the monthly medians of the
 110 $foF2$ for minimum and maximum levels of solar activity. First they found the coefficients
 111 for the Fourier time series to represent the diurnal trends of $foF2$ at about 150 ionosonde
 112 stations using Least Squares minimization method. They, then, found the coefficients
 113 for a special set of geographic functions (similar to surface waves) to describe the vari-
 114 ation of the found Fourier coefficients with geographic coordinates. As a result of their
 115 work, the diurnal and geographic variations of the monthly medians for $foF2$ are described
 116 for 2 levels of solar activity using monthly sets of coefficients.

117 In mathematical terms, the diurnal variations at a geographic latitude ϕ and East
 118 longitude θ , and at a particular universal time (UT) t expressed as angle time from π
 119 to $-\pi$, the critical frequency can be expressed as

$$foF2(\phi, \theta, t) = a_0(\phi, \theta) + \sum_{j=1}^M [a_{2i-1}(\phi, \theta) \cos(it) + a_{2i}(\phi, \theta) \sin(it)], \quad (2)$$

120 where the maximum number of the harmonics is $M = 6$, and the geographic functions
 121 a_i are defined as

$$a_i(\phi, \theta) = \sum_{j=0}^{J(0)} c_{i,j,0} P_{j,0}(\phi, \theta) + \sum_{k=1}^8 \sum_{j=0}^{J(k)} (c_{i,j,2k-1} \cos(k\phi) + c_{i,j,2k} \sin(k\phi)) \sin^j(\mu(\phi, \theta)) \cos^k(\phi), \quad (3)$$

122 where μ is a modified dip angle that can be calculated from the Earth magnetic incli-
 123 nation $I(\phi, \theta)$ as

$$\mu = \tan^{-1}(I(\phi, \theta) / \cos(\phi)). \quad (4)$$

124 The summation cutoffs $J(k)$ in Equation 3 correspond to the truncation of the higher
 125 degrees of the latitudinal expansion, introduced by Jones and Gallet (1962) to reduce
 126 the noise of the median data points. Specifically, $J = [11, 11, 8, 4, 1, 0, 0, 0, 0]$ is employed
 127 for the $foF2$.

128 Coefficients c in Equation 3 for two levels of solar activity are provided as first 1976
 129 numbers in 12 .asc files (one for each month) that accompany the IRI model.

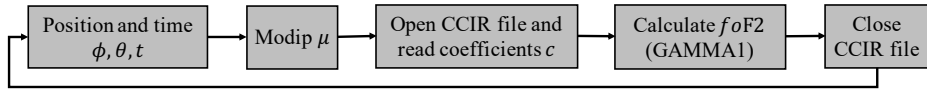


Figure 2. A simplified flow diagram of IRI model to obtain $foF2$ from CCIR coefficients.

130 In the IRI source code, a function called GAMMA1 calculates $foF2$ following Equa-
 131 tions 2 and 3. The summation is obtained by sequential multiplication and addition of
 132 the coefficients with the functions inside of FORTRAN *do* loops. A simplified version
 133 of the flow diagram for this process is shown in Figure 2. For a particular time t and ge-
 134 ographic position (ϕ, θ) , the modip μ is obtained, then the coefficients c are read from
 135 the CCIR file and the function GAMMA1 is being called to calculate $foF2$ following Equa-
 136 tion 2. For the next time frame or for the next location of interest, this same process is

137 repeated again and again. This scheme is simplified, dropping down the explanation of
 138 the interpolation between solar activity and the interpolation between 2 consequent monthly
 139 sets of coefficients.

140 3 The peak of F2 region $NmF2$: Novel approach

141 In this section a novel approach to calculate $foF2$ is described utilizing the fact that
 142 one CCIR set of coefficients contains all the necessary information to obtain the $foF2$
 143 simultaneously for the entire globe and for the entire diurnal range.

144 The starting point begins with the formation of the position 1-D arrays Φ and Θ
 145 that specify the desired global grid with number of grid points N_G . These arrays can de-
 146 scribe regular or irregular, global or regional grids. Similarly, the time of interest is spec-
 147 ified as a 1-D array T . Python 3.7 International Geomagnetic Reference Field (IGRF-
 148 13) package (Alken et al., 2021) is employed for the calculation of the magnetic inclina-
 149 tion I for the given arrays Φ and Θ , and the modip array M is further calculated using
 150 Equation 5. The global distribution of modip at zero altitude is shown in Figure 3 for
 151 Apr 1, 2020. The modip distribution specifies where the magnetic equator is on the ge-
 152 ographic coordinates.

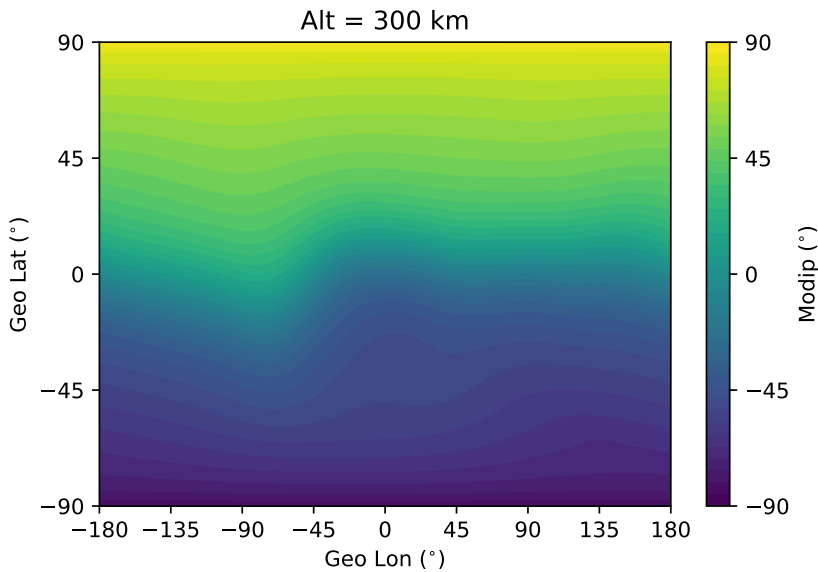


Figure 3. Example of the modified dip angle global distribution for Apr 1, 2020.

153 Next, the Fourier functions are evaluated for the given time array T . Figure 4 shows
 154 first two low order terms and the last high order terms of those functions, visualizing the
 155 highest level of the temporal resolution that can be achieved. A full list of functions is
 156 also shown on the right side of Figure 4. As a result of this step, a matrix of diurnal func-
 157 tions F_D has $[N_T, 13]$ size, where N_T is number of time steps.

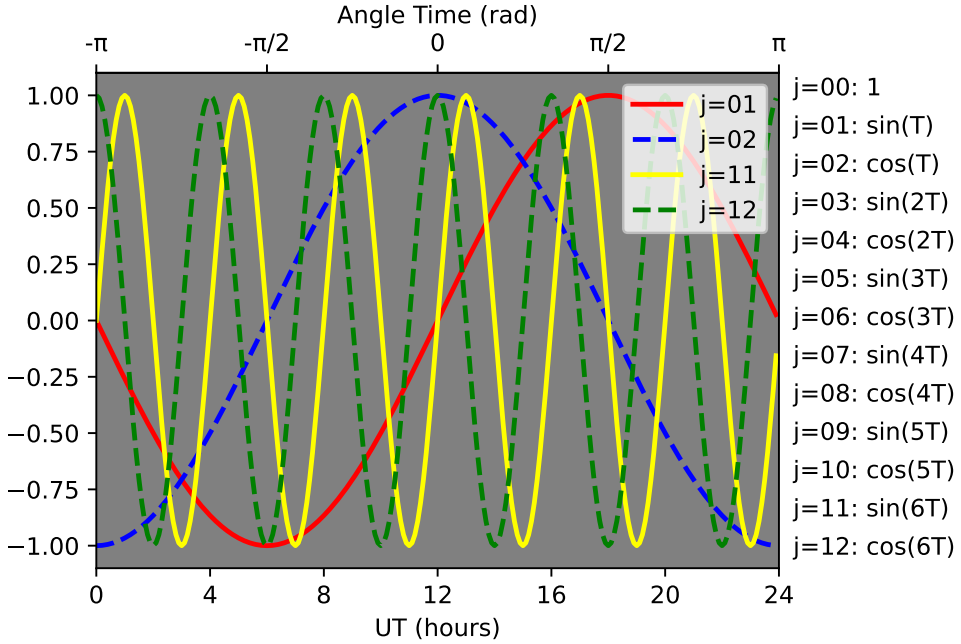
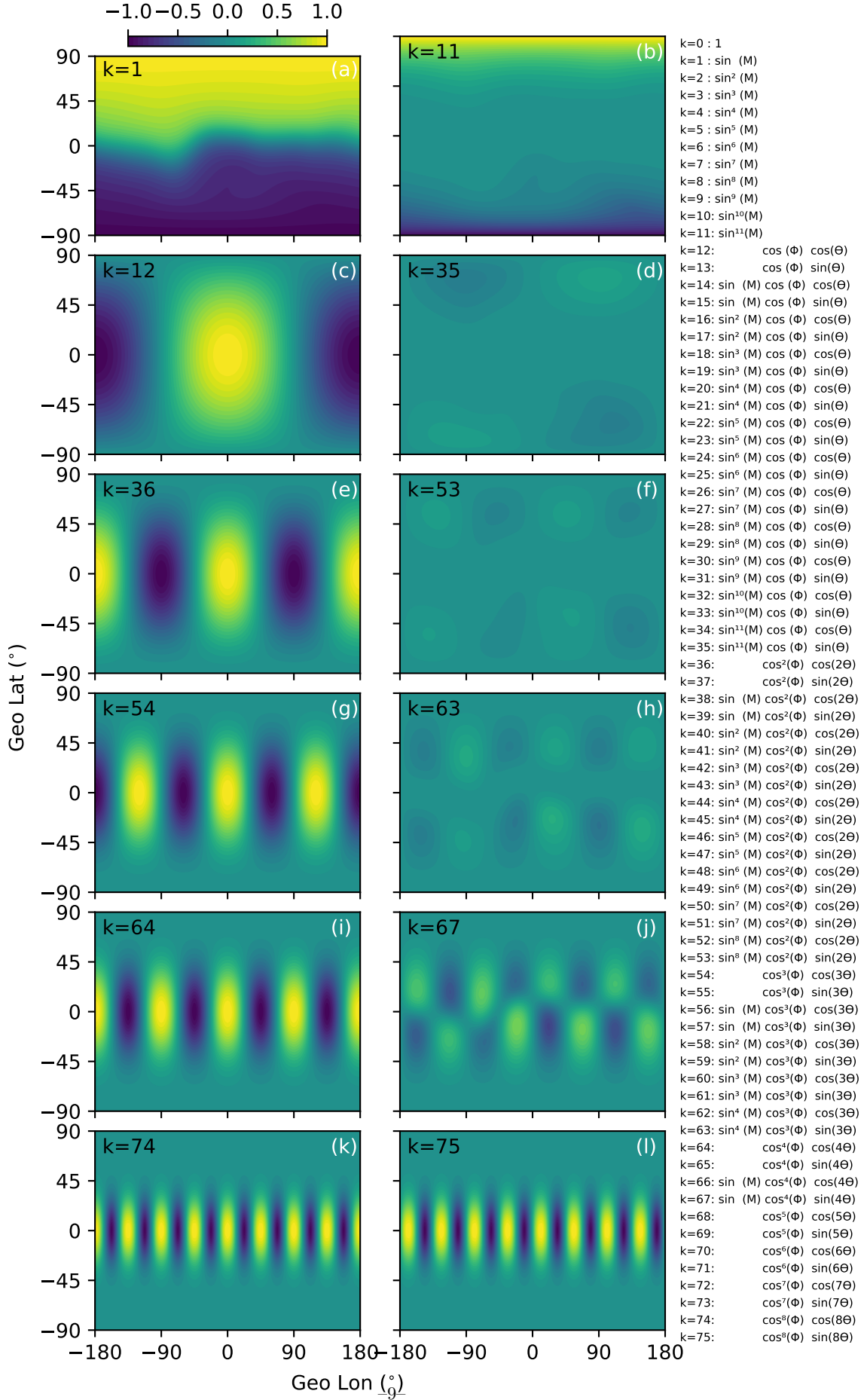


Figure 4. Few examples of the Fourier diurnal functions calculated for array of time spanned 24 hours of UT.

158 Further, the global functions are evaluated for the positional arrays Φ , Θ , and the
 159 array of modip M . Capital Greek letters are used to emphasize that these are the ar-
 160 rays and not the single numbers. Figure 5 shows several examples of the global functions.
 161 The main difference from regular spherical harmonics is the modip dependency, that can
 162 be clearly visible from the first function shown in Figure 5a. The smallest ionospheric
 163 structures that can be revealed by the highest expansion term is shown in Figure 5l. Ad-
 164 ditionally, the list of all 76 global functions is shown on the right of Figure 5. As a re-
 165 sult of this step, a matrix of global functions F_G has $[76, N_G]$ elements, where N_G is num-
 166 ber of grid points.



167 Then, the 1-D array of CCIR coefficients c that has 1976 elements can be reformed
 168 into a matrix U of size [13, 76, 2], where the first dimension corresponds to 13 Fourier
 169 series, the second dimension represents 76 global functions, and the third dimension rep-
 170 presents the 2 levels of solar activity. For one level of solar activity matrix U is reduced
 171 to size [13, 76].

172 Finally, a matrix multiplication operation

$$foF2 = (F_D U) F_G \quad (5)$$

173 gives a critical frequency $foF2$ matrix with size $[N_T, N_G]$, which is further converted to
 174 $NmF2$ using Equation 1.

175 An example of the $NmF2$ output for 2 levels of solar activity is shown in Figure
 176 6 for 10 UT of April 15, 2020. The location of the subsolar point is shown with red cir-
 177 cle. For the solar minimum, the CCIR coefficients were derived using data from 1954-
 178 1955, and for the solar maximum the years 1956-1958 were considered (Jones & Gallet,
 179 1962, 1965; Jones et al., 1969).

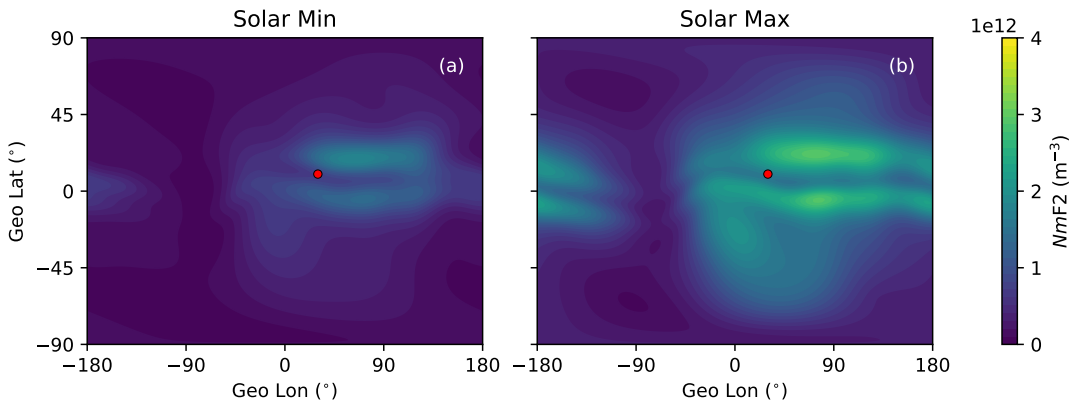


Figure 6. Peak of electron density $NmF2$ for solar minimum (a) and solar maximum (b) for 10 UT of April 2020. Red circle shows the location of subsolar point.

180 A simplified version of the flow diagram for the PyIRI code is shown in Figure 7.
 181 In summary, the global functions F_G are calculated for 3 arrays Φ , Θ , and M , and the
 182 Fourier functions F_T are calculated for a time array T . The CCIR coefficients are stored
 183 in matrix U , and the multiplication between F_D , U , and F_G gives $foF2$ for the entire
 184 grid and for the entire time array. Importantly, this one operation substitutes 6,272,736

185 executions of the IRI FORTRAN code in case of global regular grid of $1^\circ \times 1^\circ$ and 15-
 186 min-resolution temporal array.

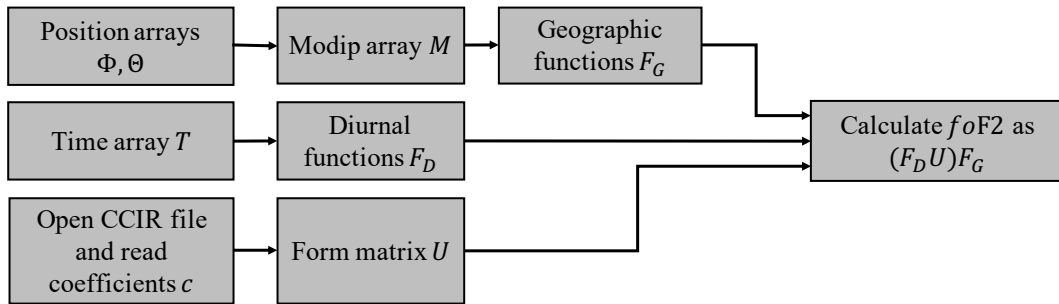


Figure 7. A simplified flow diagram for the PyIRI code to obtain $foF2$ from CCIR coefficients.

187 4 The height of F2 peak $hmF2$

188 The CCIR files also contain 882 coefficients (following first 1976 coefficients for $foF2$)
 189 that correspond to the $MUF(3000)F2/foF2$, where $MUF(3000)F2$ is the highest frequency
 190 that is refracted in the ionosphere and can be received at a distance of 3,000 km. The
 191 only difference between the calculation of $foF2$ and $MUF(3000)F2/foF2$ is in the num-
 192 ber of the global and diurnal functions. In the case of $MUF(3000)F2/foF2$, the trun-
 193 cation is determined by $J = [6, 7, 5, 2, 1, 0, 0]$ and gives 49 geographic functions, whereas
 194 9 Fourier functions are used. Therefore, the matrix with the CCIR coefficients has $[9, 49, 2]$
 195 size. Figure 8 shows $MUF(3000)F2/foF2$ for minimum and maximum solar activity cal-
 196 culated from CCIR coefficients for April of 2020, 10 UT.

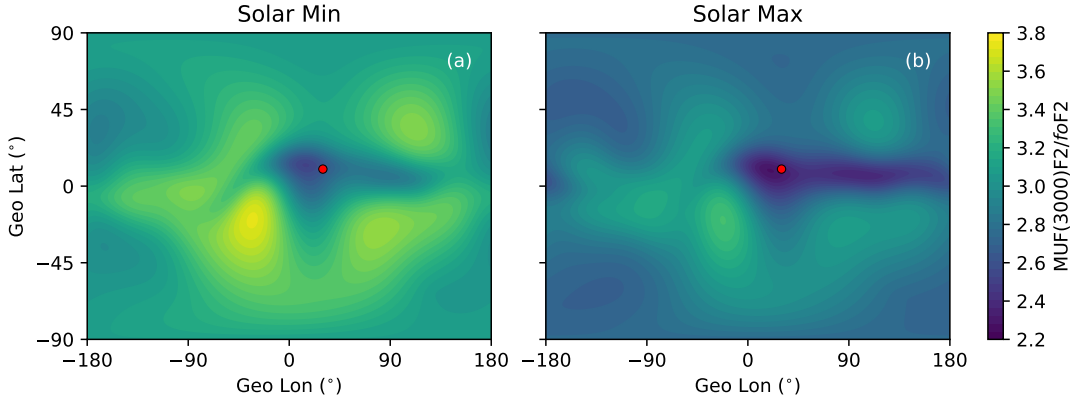


Figure 8. CCIR MUF(3000)F2/foF2 for solar minimum (a) and solar maximum (b) for 10 UT of April 2020. Red circle shows the location of subsolar point.

197 Further, following BSE-1979 option of IRI (Bilitza et al., 2022), developed by Bilitza
198 et al. (1979) the $hmF2$ parameter is derived as

$$hmF2 = \frac{1490}{MUF(3000)F2/foF2 + DM} - 176, \quad (6)$$

199 where the correction factor DM is

$$DM = \frac{f_1 f_2}{\frac{foF2}{foE} - f_3} + f_4, \quad (7)$$

200 and the following functions f depend on 12-month running mean of sunspot number R_{12}
201 and on modip array M

$$f_1 = 0.00232R_{12} + 0.222, \quad (8)$$

$$f_2 = 1 - \frac{R_{12}}{150} \exp \left[- \left(\frac{M}{40} \right)^2 \right], \quad (9)$$

$$f_3 = 1.2 - 0.0116 \exp \left(\frac{R_{12}}{41.84} \right), \quad (10)$$

$$f_4 = 0.096 \frac{R_{12} - 25}{150}. \quad (11)$$

205 An additional limit is added to ratio $\frac{foF2}{foE}$, where it is fixed at 1.7 in case it goes below
206 1.7.

207 After applying Equation 6, the height of the F2 region peak is shown in Figure 9.

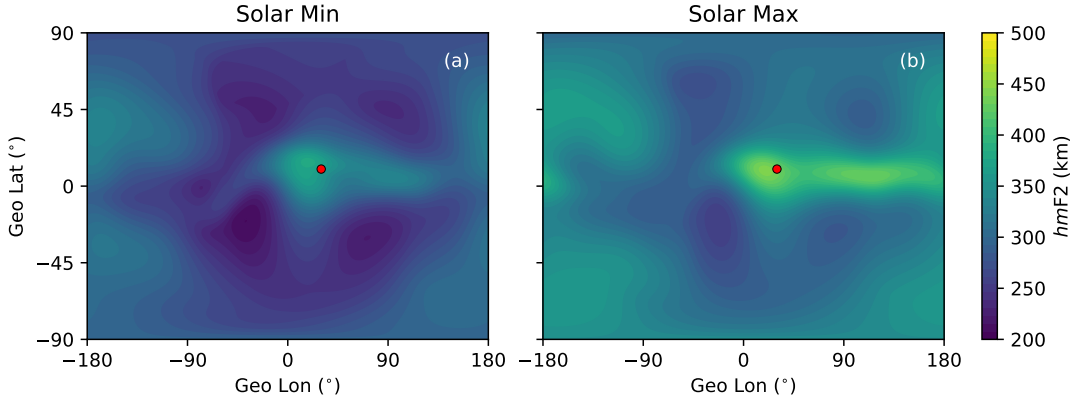


Figure 9. Height of the electron density peak $hmF2$ for solar minimum (a) and solar maximum (b) for 10 UT of April 2020. Red circle shows the location of subsolar point.

208 5 E region parameters

209 The E region model for this version of PyIRI was chosen to be somewhat simpler
 210 than the one used in the source code of IRI, following the approach from NeQuick model.
 211 First the effective solar zenith angle is being calculated as

$$\Psi_{eff} = \frac{\Psi + [90 - 0.24 \exp(20 - 0.2\Psi)] \exp(12(\Psi - \Psi_0))}{1 + \exp(12(\Psi - \Psi_0))}, \quad (12)$$

212 where Ψ is a solar zenith angle, and Ψ_0 is a solar zenith angle at day night transition,
 213 which is set to 86.23292796211615° .

214 Further a seasonal parameter s is defined as

$$s = s_0 \left(\frac{\exp(0.3\Phi) - 1}{\exp(0.3\Phi) + 1} \right), \quad (13)$$

215 with s_0 being month dependent

$$s_0 = \begin{cases} -1, & \text{month } = 1, 2, 11, 12, \\ 0, & \text{month } = 3, 4, 9, 10, \\ 1, & \text{month } = 5, 6, 7, 8. \end{cases} \quad (14)$$

216 The critical frequency of E region is then calculated using

$$foE = \sqrt{0.49 + (1.112 - 0.019s)^2 \sqrt{F10.7} \cos^{0.6}(\Psi_{eff})}, \quad (15)$$

217 where $F10.7$ is the solar radio flux at 10.7 cm, and Ψ_{eff} is converted to radians.

218 Figure 10 shows the *E*-region critical frequency for 2 levels of solar activity for 10
 219 UT of April 2020. The climatology of E region is mainly controlled by the solar ioniza-

220 tion and therefore depends on the location of subsolar point, shown with red circle in
 221 Figure 10.

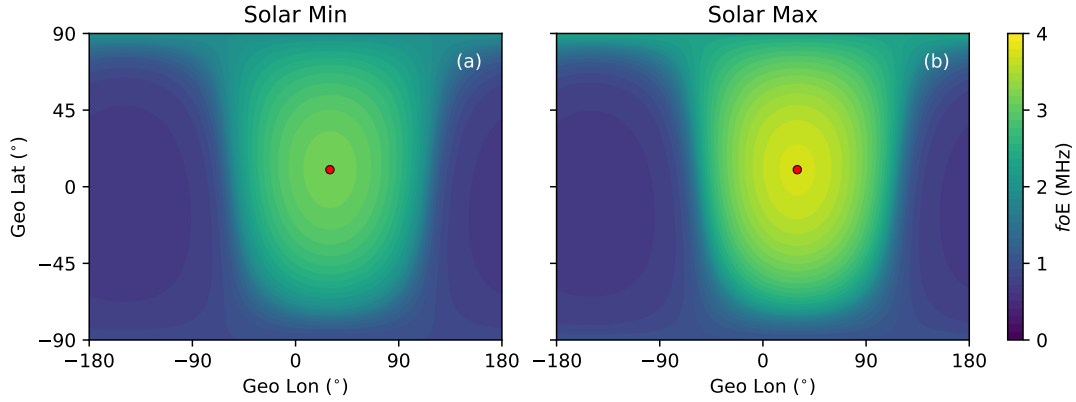


Figure 10. f_{0E} for solar minimum (a) and solar maximum (b) for 10 UT of April 2020. Red circle shows the location of subsolar point.

222 Additionally, the height of the E region hmE is assumed to be fixed at 110 km, with
 223 the thickness of the bottom side of E region B_{bot}^E being fixed at 5 km, and B_{top}^E being
 224 fixed at 7 km.

225 6 Thicknesses of the ionospheric layers

226 This version of the PyIRI code has simplified approach to the construction of the
 227 ionospheric profile, in comparison to the standard IRI source code and its options. For
 228 the thickness of bottom side of F2 region, an approach similar to NeQuick model is cho-
 229 sen, where the bottom side is being described by Epstein function, that has one param-
 230 eter that describes it's thickness, unlike the IRI model, where two parameters B_0 and
 231 B_1 are employed.

232 6.1 Thickness of the bottom side of the F2 layer B_{bot}^{F2}

233 The thickness of the bottom layer in PyIRI is modeled as a function of f_{0F2} and
 234 MUF(3000)F2/ f_{0F2} as

$$235 B_{bot}^{F2} = \frac{47.74}{\exp(-3.467 + 1.714 \ln(f_{0F2}) + 2.02 \ln(\text{MUF}(3000)F2/f_{0F2}))}, \quad (16)$$

236 and is shown in Figure 11 for 2 levels of solar activity.

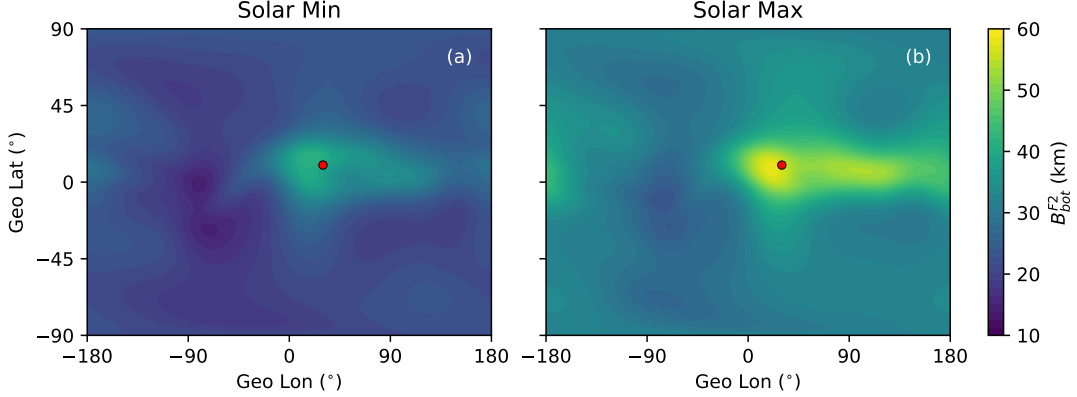


Figure 11. Thickness of the bottom side of F2 region B_{bot}^{F2} for solar minimum (a) and solar maximum (b) for 10 UT of April 2020. Red circle shows the location of subsolar point.

6.2 Thickness of the top side of the F2 layer

IRI model provides three different options to define the thickness of the top side of F2 layer B_{top}^{F2} , with the NeQuick approach being the standard option. However, there are slight differences in the definitions B_{top}^{F2} in NeQuick and IRI code. Here we define B_{top}^{F2} the following way, combining the two approaches:

$$B_{top}^{F2} = \frac{100x + 150}{0.041163x^2 - 0.183981x + 1.424472}, \quad (17)$$

where x depends on B_{bot}^{F2}

$$x = \frac{kB_{bot}^{F2} - 150}{100}, \quad (18)$$

with shape parameter k defined as

$$k = 3.22 - 0.0538foF2 - 0.00664hmF2 + 0.113\frac{hmF2}{B_{bot}^{F2}} + 0.00257R_{12}. \quad (19)$$

In NeQuick definition of k , the dependence on the solar activity is expressed in terms of effective ionization level, whereas in IRI the 12-month running-mean of sunspot number R_{12} is used. The B_{top}^{F2} is shown in Figure 12 for 2 levels of solar activity.

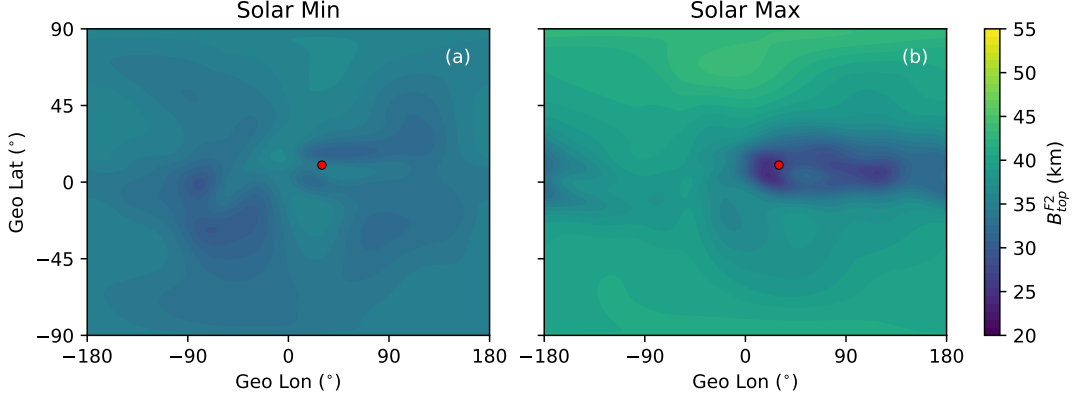


Figure 12. Thickness of the top side of F2 region B_{top}^{F2} for solar minimum (a) and solar maximum (b) for 10 UT of April 2020. Red circle shows the location of subsolar point.

7 F1 region parameters

The F1 region appears only during the day time. It's occurrence probability function

$$P = (0.5 + 0.5 \cos(\Psi))^{2.36}, \quad (20)$$

was chosen not to depend on R_{12} and magnetic latitude, following the suggestion in Bilitza et al. (2022). The distribution of P is shown in Figure 13a, with the color bar shown on the right of the figure. It's global distribution is very similar to the NmE distribution, indicating strong solar control. Further, when the occurrence probability is greater than 0.5, the critical frequency of F1 layer can be modeled as

$$foF1 = f_s \cos^n(\Psi), \quad (21)$$

where

$$\begin{aligned} f_s &= f_0 + \frac{(f_{100} - f_0)R_{12}}{100}, \\ f_0 &= 4.35 + 0.0058|M'| - 0.00012M'^2, \\ f_{100} &= 5.348 + 0.011|M'| - 0.00023M'^2, \\ n &= 0.093 + 0.0046|M'| - 0.000054M'^2 + 0.0003R_{12}, \\ M' &= \tan^{-1}\left(\frac{1}{2} \tan(M)\right), \end{aligned} \quad (22)$$

with M' being magnetic dip latitude, that can be calculated from modified dip angle matrix M . Figures 13b and 13c show the critical frequency $foF1$ during solar minimum and solar maximum, respectively, for 10 UT of April 2020.

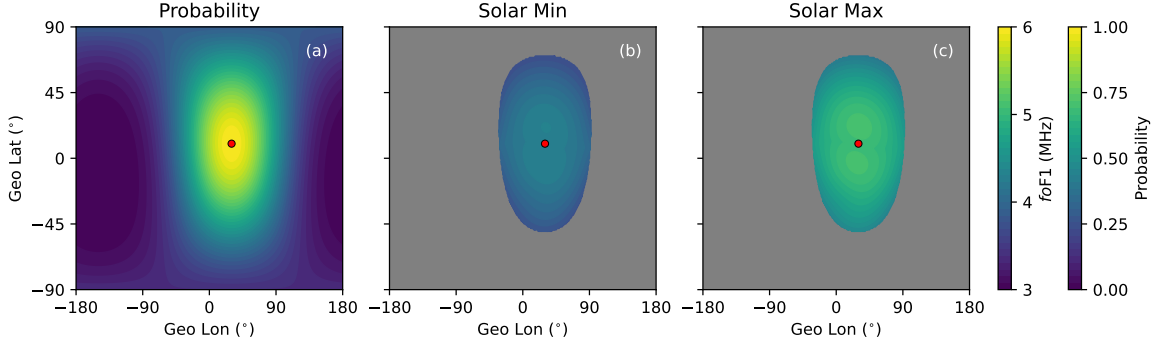


Figure 13. Occurrence probability function P for F1 region (a), with critical frequency $foF1$ during solar minimum (b) and solar maximum (c) for 10 UT of April 2020. Red circle shows the location of subsolar point.

258 The height of the F1 layer $hmF1$ is found where the bottom side of F2 layer drops
 259 to the value of $foF1$, in case when F1 layer is present. This height is found analytically
 260 using the following expression derived from Epstein function

$$hmF1 = B_{bot}^{F2} \log \left(- \left(1 - \frac{2NmF2}{NmF1} \right) - \sqrt{\left(1 - \frac{2NmF2}{NmF1} \right)^2 - 1} \right) + hmF2. \quad (23)$$

261 The $hmF1$ map is shown in Figure 14.

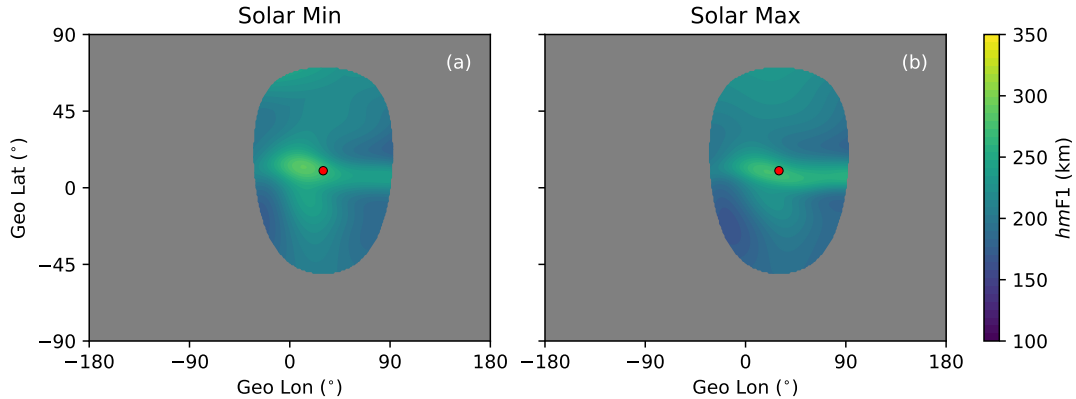


Figure 14. F1 region peak height $hmF1$ during solar minimum (a) and solar maximum (b) for 10 UT of April 2020. Red circle shows the location of subsolar point.

262 A regular Epstein function is employed to model the bottom side of F1 region, with
 263 the following thickness

$$B_{bot}^{F1} = 0.5(hmF1 - hmE), \quad (24)$$

264 that is also shown in Figure 15.

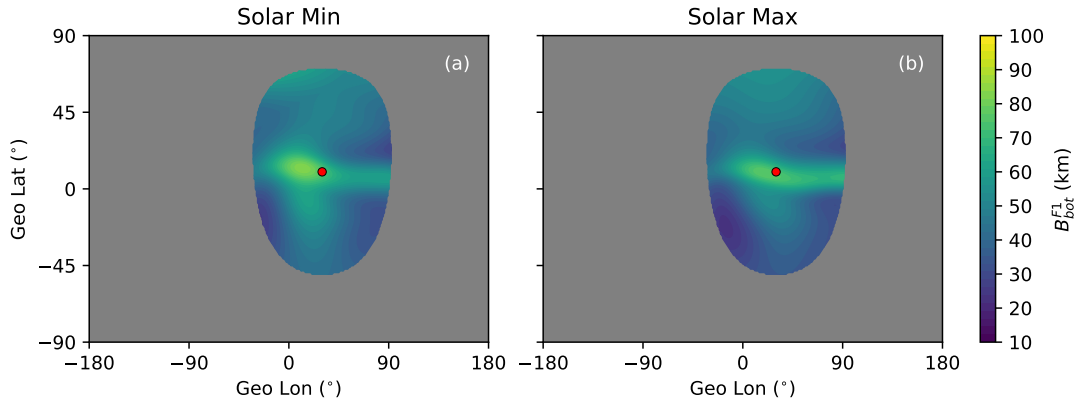


Figure 15. Thickness of the bottom side of F1 region B_{bot}^{F1} for solar minimum (a) and solar maximum (b) for 10 UT of April 2020. Red circle shows the location of subsolar point.

265 **8 Sporadic E layer *Es***

266 PyIRI also includes monthly mean of the sporadic E layer *Es*, using mean monthly
 267 coefficients (Bradley, 2003). They are in the same format as CCIR coefficients, but with
 268 different truncation of the higher degrees of the latitudinal expansion $J = [10, 12, 6, 2, 0, 0]$.
 269 Figure 16 shows the critical frequency of the sporadic E layer *Es* for both levels of so-
 270 lar activity.

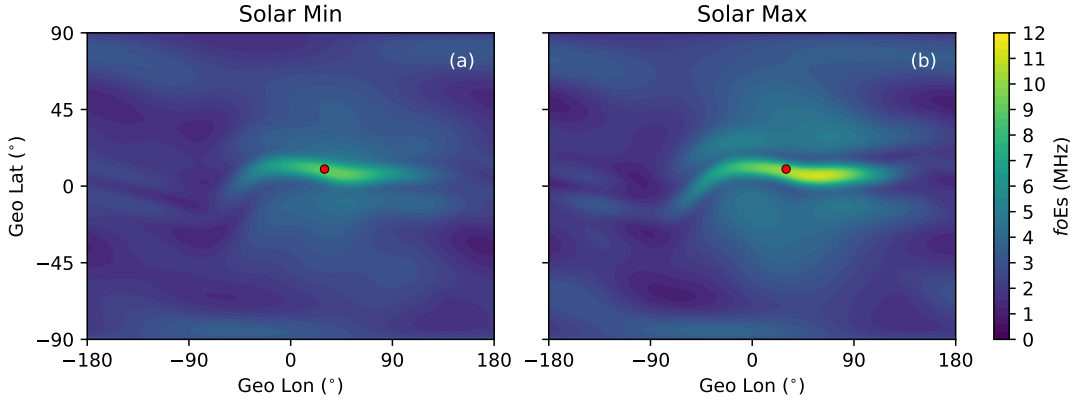


Figure 16. Critical frequency of the sporadic E layer E_s for solar minimum (a) and solar maximum (b) for 10 UT of April 2020. Red circle shows the location of subsolar point.

271 This parameter, however, is not included in the construction of the vertical elec-
272 tron density profile, described in the following section.

273 9 Construction of the 3-D ionosphere from the maps of the param- 274 eters

275 This section explains how the 3-D ionosphere is constructed form the maps of the
276 ionospheric parameters. This approach was specifically developed for PyIRI.

277 First, let's consider a 1-D example of the profile construction from the set of co-
278 efficients. The coefficients were chosen from the $\phi = 0^\circ$ and $\theta = 100^\circ$ location, where
279 the F1 region is not present, for solar maximum condition. Figure 17a shows the $NmF2$
280 and NmE parameters with red and purple circles, located at the $hmF2$ and hmE heights,
281 respectively.

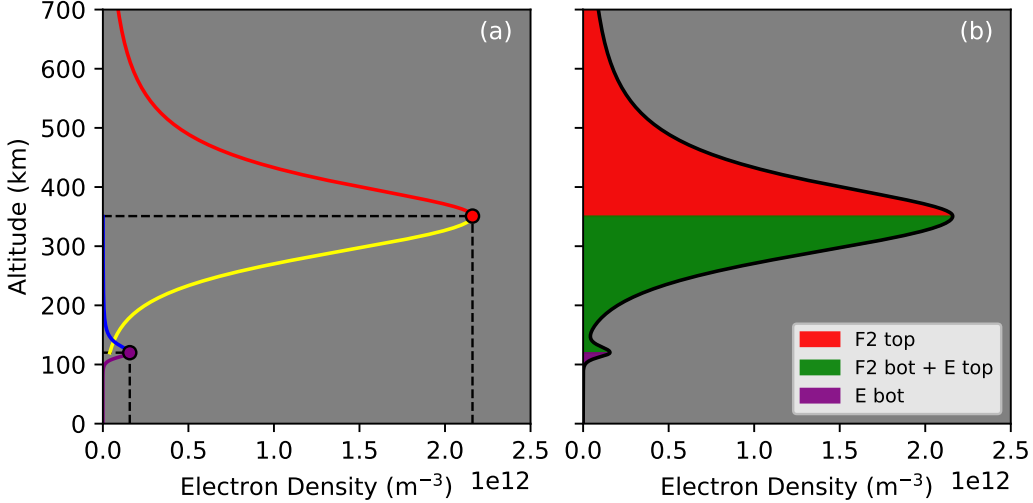


Figure 17. Construction of the EDP without F1 region.

The bottom side of the F2 region, the topside of E region, and the bottom side of E region, shown with yellow, blue, and purple colors in Figure 17a are constructed using Epstein function

$$Ne = 4Nm \frac{e^{\frac{h-hm}{B}}}{\left(1 - e^{\frac{h-hm}{B}}\right)^2}, \quad (25)$$

using corresponding peak densities Nm , heights of the peaks hm , and thicknesses B . The bottom side of F2 region is evaluated from $hmF2$ down to hmE . The topside of E region is evaluated from hmE up to $hmF2$. Further, the top side of the F2 region, shown with red in Figure 17 is calculated using Equation 25, with the modified thickness of the profile

$$B_{modified} = B_{top}^{F2} \left(1 + \frac{12.5(h - hmF2)}{100B_{top}^{F2} + 0.125(h - hmF2)}\right). \quad (26)$$

A special care needs to be taken for the region between $hmF2$ and hmE to add two curves together. Unlike in IRI and NeQuick, a drop function was introduced to model the transition of E region to the F2 region, without any re-scaling of the peaks. A drop function of the following form was implemented

$$Y_{up} = 1 - \left(\frac{h - hmE}{hmF2 - hmE}\right)^4. \quad (27)$$

Prior to the summation, the topside of E region is multiplied by Y_{up} and the bottom side of F2 is multiplied by

$$Y_{down} = 1 - \left(\frac{hmF2 - h}{hmF2 - hmE}\right)^4. \quad (28)$$

296 Since the contribution of the E region is minimal above 150 km, the shape of the bot-
 297 tom side F2 region remains unchanged, but the influence of the F2 region on the top-
 298 side of E region will be reduced. Figure 17b shows the final profile with different regions
 299 indicated by the color.

300 In case when the F1 region is present, like at the location with $\phi = 0^\circ$ and $\theta =$
 301 0° , the bottom side of F1 region is modeled as an Epstein function, and the bottom of
 302 the F2 region is not extended further than $hmF1$. The same drop function is used to re-
 303 duce the influence of F1 region on the top side of E region and the influence of the top
 304 of E region on the bottom of F1 region prior to their summation. Figure 18a shows the
 305 $NmF1$ with orange circle and the bottom of the F1 region with yellow curve. As can be
 306 seen in Figure 18b, the drop function approach works well to merge the 2 regions with-
 307 out changing the shapes of the individual regions and without any re-scaling of the peaks.

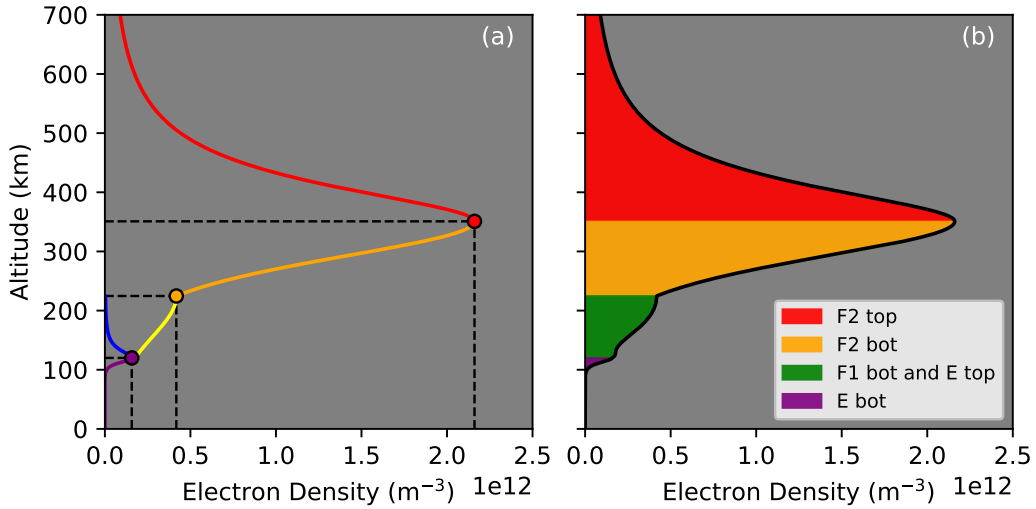


Figure 18. Construction of the EDP with F1 region.

308 It is important to mention, that even if the computation time was dramatically re-
 309 duced to construct the maps of $NmF2$ and $hmF2$ from the CCIR coefficients and to fur-
 310 ther derive all the other parameters in matrix form, it would still be computationally ex-
 311 pensive to build the profiles in the traditional way, by doing it for each horizontal po-
 312 sition. In this case, a particular function that constructs the profiles from the set of co-
 313 efficients would need to be (again, on top of the derivation of the parameters) called 6, 272, 736

314 times in case of the global regular grid of $1^\circ \times 1^\circ$ and 15-min-resolution temporal ar-
 315 ray.

316 This problem, however, can be solved with the help of Python *numpy.where* func-
 317 tion in NumPy package that can have not only multidimensional argument, but also a
 318 multidimensional condition. Figure 19 helps to visualize this 2-D selection, where red,
 319 orange, and purple surfaces show $hmF2$, $hmF1$, and hmE , respectively. These surfaces
 320 represent the boundaries for the selection, similar to 1-D example with red, orange and
 321 purple circles in Figure 18a. For example, to construct the topside of the ionosphere si-
 322 multaneously for the entire global grid, all 3-D grid points that are located above the
 323 red surface need to be selected and passed to the Epstein function. Similarly, to construct
 324 the bottom side of the F2 region, when the F1 region is present, all the points between
 325 the green and red surfaces should be selected. The trick to make a 2-D selection is to
 326 present all parameters as 2-D matrices, by populating the same information at all heights.
 327 For example, a matrix for $hmF2$ will have $[N_G, N_V]$ size, where N_V is the number of de-
 328 sired vertical grid cells that correspond to an array of altitudes h . This matrix will have
 329 same elements at all N_V . Same should be done for all other parameters. However, the
 330 height matrix H should have $[N_V, N_G]$ elements, with the heights being equal at all hor-
 331 izontal locations. Further, the output of *numpy.where*($H \geq hmF2$) gives 2-D indexes
 332 for the location of all the grid cells that correspond to the ionospheric top side of F2 re-
 333 gion IND_{top}^{F2} . Finally, $NmF2[IND_{top}^{F2}]$, $hmF2[IND_{top}^{F2}]$, $B_{top}^{F2}[IND_{top}^{F2}]$, and $H[IND_{top}^{F2}]$
 334 can be given to the topside Epstein function using Equations 25 and 26 to perform the
 335 calculation of the electron density for the top side of the F2 region. The result will have
 336 the same shape $[N_G, N_V]$ as the input.

337 Additionally, it is not necessary to introduce a separate dimension for time with
 338 size N_T . Instead, all the matrices can have $[N_G \times N_T, N_V]$ shape and the final outputs
 339 can be further reshaped to $[N_T, N_G, N_V]$.

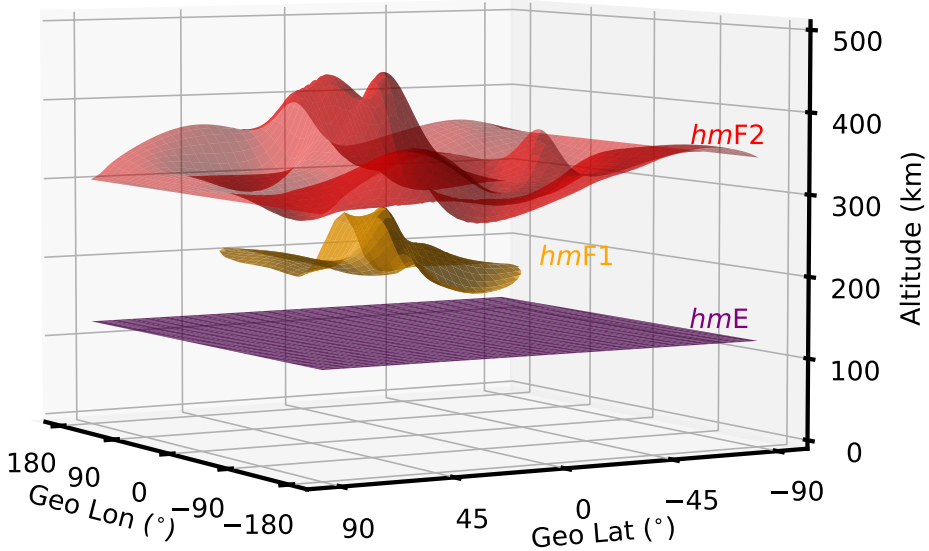


Figure 19. Surfaces of $hmF2$, $hmF1$, and hmE parameters that represent the boundaries for the 2-D selection of the 3-D grid points.

10 Solar and seasonal interpolation

All the ionospheric parameters are being determined for two solar reference points, i.e. solar minimum condition and solar maximum condition, whereas all the parameters represent monthly mean values. Therefore, to estimate electron density for a particular day of the year, the interpolation in solar activity and in day of the month needs to be performed.

To find the ionospheric parameters (let's call them P) for a particular day-of-the month, the mean parameters are found for the two consequent months around the day of interest. In case the day of interest is less than the 15th of the month, the month before P_1 and the current month P_2 will be taken as a reference points. In case the day of interest is greater than 15, the current month P_1 and the following month P_2 are con-

351 sidered. The following expression is used for the interpolation

$$P = P_1 f_2 + P_2 f_1, \quad (29)$$

352 where f_1 is a ratio of number of days between the day of interest and the middle of the
 353 month that corresponds to P_2 , whereas f_2 is the ratio of number of days between the day
 354 of interest and the middle of the month that corresponds to P_1 . This is how a smooth
 355 transition in between the middles of the months is obtained.

356 In the original studies of Jones and Gallet (1962, 1965), the CCIR coefficients were
 357 determined for years 1954–1955 representing solar minimum conditions with $R12=0$ and
 358 1956–1958 for the solar maximum with $R12=100$. Further, it was found that better re-
 359 sults can be achieved if solar maximum coefficients correspond to $IG12_{min} = 0$, and
 360 solar maximum to $IG12_{max} = 100$ (R. Ma, 1983; Liu & Chen, 2009; R. Ma, 2009).

361 PyIRI uses F10.7 as a solar driver, but the interpolation between solar minimum
 362 and solar maximum is determined based on IG12 coefficient. First the F10.7 of the day
 363 of interest is converted to R12 and then from R12 to IG12. The following quadratic equa-
 364 tions are used for the conversion

$$IG12 = -0.00268R12^2 + 1.468R12 + 12.349, \quad (30)$$

365

$$F107 = 0.00089R12^2 + 0.728R12 + 63.7. \quad (31)$$

366 Linear interpolation for all ionospheric parameters is further obtained in matrix form us-
 367 ing

$$P = \frac{P_{min}(IG12_{max} - IG12) + P_{max}(IG12 - IG12_{min})}{IG12_{max} - IG12_{min}}, \quad (32)$$

368 where $IG12$ for the day of interest is derived from F10.7 using Equations 30 and 31.

369 11 PyIRI Tool

370 PyIRI can be downloaded using the following command in a terminal window

`pip3 install PyIRI`

371 Any Python environment can be used to run PyIRI, where `.py` file is placed into
 372 `/PyIRI/Code/` directory. Initially, all the necessary libraries need to be installed as

```
import PyIRI_Library as ml
import PyIRI_IGRF_Library as IGRF
import PyIRI_Plottting_Library as plot
```

373 after which, they can be called as `ml.`, `IGRF.`, and `plot..`

374 To obtain the ionospheric parameters and the electron density for a particular day,
 375 the following command in Python can be used:

```
F2, F1, E, Es, sun, mag, EDP=ml.IRI_density_1day(year, month, day, aUT,
                                                    alon, alat, aalt, F107, dir)
```

376 where the inputs `year`,`month`,`day` are integers, and `aUT`,`alon`,`alat`,`aalt` are 1-D NumPy
 377 arrays with sizes $[N_T]$, $[N_G]$, $[N_G]$, $[N_V]$, and units of (hours), ($^{\circ}$), ($^{\circ}$), and (km), respec-
 378 tively. They can be regularly or irregularly spaced. `F107` can be used to provide the so-
 379 lar driver, whereas in case `numpy.nan` is assigned to this parameter, the `F10.7` will be
 380 taken from OMNIWeb data file located at `/PyIRI/Solar_Drivers/`. Lastly, `dir` should
 381 be a string direction of `PyIRI` folder on your machine.

382 The outputs `F2`,`F1`,`E`,`Es` are the dictionaries with the ionospheric parameters `Nm`,
 383 `hm`, `fo`, `B_top`, and `B_bot`. `F2` dictionary also includes `M3000` parameter, and `F1` dictio-
 384 nary also includes probability density `P` for the occurrence of `F1` region. All are param-
 385 eters have size $[N_T, N_G]$. `EDP` is electron density of size $[N_T, N_V, N_G]$ expressed in (m^{-3}).
 386 `sun` dictionary contains `lon` and `lat` for subsolar point location in ($^{\circ}$), with size $[N_T]$.
 387 `mag` dictionary includes magnetic inclination `inc` in ($^{\circ}$), modified dip angle `modip` in ($^{\circ}$),
 388 and magnetic dip latitude `mag_dip_lat` in ($^{\circ}$), all of size $[N_G]$.

389 In case one is interested in monthly mean parameters for minimum and maximum
 390 levels of solar activity, the following command can be used:

```
F2, F1, E, Es, sun, mag=ml.IRI_monthly_mean_parameters(year, month, aUT, alon, alat, dir)
```

391 in which case, the output arrays in the dictionaries `F2`,`F1`,`E`,`Es` will have size $[N_T, N_G, 2]$,
 392 where the last dimension indicates 2 levels of solar activity. Further, the monthly mean
 393 electron density can be constructed using

```
EDP=ml.reconstruct_density_from_parameters(F2, F1, E, aalt)
```

394 where the output has shape $[2, N_T, N_V, N_G]$. An example of how PyIRI can be used is
 395 included in `/PyIRI/Code/PyIRI.py` or `/PyIRI/Code/PyIRI.ipny` that can be opened
 396 with Jupyter Notebook.

397 12 Conclusion

398 This paper presented a novel approach for the empirical modeling of the ionosphere
 399 that allows the evaluation of the model parameters simultaneously on the entire global
 400 grid and for the entire diurnal time array using well-known and validated CCIR coef-
 401 ficients. The derivation of other ionospheric parameters, that depend on CCIR maps,
 402 were described. A novel approach to the construction of the vertical electron density pro-
 403 files for the entire diurnal and global grid was introduced. Finally, examples of how the
 404 open-source Python tool PyIRI can be used were provided.

405 13 Open Research

406 PyIRI software is made available to the community.

407 Acknowledgments

408 The IRI homepage at <http://irimodel.org> provides open access to the FORTRAN model
 409 code of all major version of the model, to online computations of IRI parameters, and
 410 to information about IRI members, workshops, and publications. OMNI data is avail-
 411 able through <https://omniweb.gsfc.nasa.gov/form/dx1.html>.

412 References

- 413 Alken, P., Thébault, E., Beggan, C. D., & et al. (2021). International geomagnetic
 414 reference field: the thirteenth generation. *Earth, Planets and Space*, 73(49).
 415 doi: 10.1186/s40623-020-01288-x
- 416 Bilitza, D., Pezzopane, M., Truhlik, V., Altadill, D., Reinisch, B. W., & Pignal-
 417 beri, A. (2022). The international reference ionosphere model: A review
 418 and description of an ionospheric benchmark. *Rev. Geophys.*, 60(4). doi:
 419 10.1029/2022RG000792
- 420 Bilitza, D., Sheik, N., & Eyfrig, R. (1979). A global model for the height of the f2-
 421 peak using m3000 values from the ccir numerical map. *ITU Telecommunication
 422 Journal*, 46, 549-553.

- 423 Bradley, P. (2003). Ingesting a sporadic-e model to iri. *Adv. Space Res.*, 31(3), 577-
424 588.
- 425 Jones, W. B., & Gallet, R. M. (1962). Representation of diurnal and geographic
426 variations of ionospheric data by numerical methods. *Journal of Research
427 of the National Bureau of Standards*, 66(4), 129–147. doi: 10.6028/jres.066D
428 .043
- 429 Jones, W. B., & Gallet, R. M. (1965). Representation of diurnal and geographic
430 variations of ionospheric data by numerical methods, ii. control of instability.
431 *ITU Telecommunication Journal*, 32(1), 18–28.
- 432 Jones, W. B., Graham, R. P., & Leftin, M. (1969). *Advances in ionospheric mapping
433 by numerical methods*.
- 434 Liu, L., & Chen, Y. (2009). Statistical analysis of solar activity variations of total
435 electron content derived at Jet Propulsion Laboratory from GPS observations.
436 *J. Geophys. Res.*, 114. doi: 10.1029/2009JA014533
- 437 Nava, B., Coïsson, P., & Radicella, S. (2008). A new version of the nequick iono-
438 sphere electron density model. *J. Atmos. Sol. Terr. Phys.*, 70(15), 1856–1862.
439 doi: 10.1016/j.jastp.2008.01.015
- 440 R. Ma, W. W. W. Y., j. Xu. (1983). A new solar index which leads to improved fof2
441 predictions using the ccir atlas. *Telecommunication Journal*, 50(8), 408-414.
- 442 R. Ma, W. W. W. Y., j. Xu. (2009). Seasonal and latitudinal differences of the sat-
443 uration effect between ionospheric nmf2 and solar activity indices. *J. Geophys.
444 Res.*, 114(A10).